IEEE Access
Multidisciplinary ⋮ Rapid Review ⋮ Open Access Journal

Received March 21, 2019, accepted April 4, 2019, date of publication May 20, 2019,
date of current version December 23, 2020.

Digital Object Identifier 10.1109/ACCESS.2019.2917931

Simulation Performance Enhancement in Automotive Embedded Control Using the Unscented Transform

ABRAHAM ELIAS ORTEGA PAREDES[1], LAURO ROBERTO NUNES[1], MAX MAURO DIAS SANTOS[1], (Senior Member, IEEE), LEONARDO RODRIGUES ARAÚJO XAVIER DE MENEZES[2], (Member, IEEE), KATHYA SILVIA COLLAZOS LINARES[3], JOÃO FRANCISCO JUSTO[4], AND ZONGHUA GU[5], (Senior Member, IEEE)

[1]Departamento de Eletrônica, Universidade Tecnológica Federal do Paraná, Ponta Grossa 84016-210, Brazil
[2]Departamento de Engenharia Elétrica, Universidade de Brasília, Brasília 70919-970, Brazil
[3]Departamento de Informática, Universidade Tecnológica Federal do Paraná, Pato Branco 85503-390, Brazil
[4]Escola Politécnica, Universidade de São Paulo, São Paulo 05424-970, Brazil
[5]Department of Applied Physics and Electronics, Umea University, 901 87 Umea, Sweden

Corresponding author: Max Mauro Dias Santos (maxsantos@utfpr.edu.br)

This work was supported by the Universidade Tecnológica Federal do Paraná—Ponta Grossa (UTFPR-PG).

ABSTRACT Automotive embedded systems comprise several domains, such as in software, electrical, electronics, and control. When designing and testing functions at the top level, one generally ignores the uncertainties arising from the electrical and electronic effects, which could lead to an irregular behavior and deteriorate their performance even using the appropriate methodology for designing the embedded control systems. Then, the studies and comparison on the effect of uncertainty in the automotive domain are important to improve the overall performance of those control systems. Here, we explored the uncertainty in control systems using the Monte Carlo (MC) and unscented transform (UT) methods. These methods have been applied to a mobile seat platform (MSP) and a light emitting diode (LED) used for lighting of heavy-duty vehicles. The UT for embedded control systems has shown better performance when compared to the Monte Carlo method, in order to reduce the number of required variables and computational resources in the simulation of failures and test-case generation. Finally, this investigation brings another application for the UT, in order to exemplify its applicability and advantages when compared with the other methods.

INDEX TERMS Automotive, unscented transform, Monte Carlo and embedded system.

I. INTRODUCTION

The statistical distribution with a small data sample could still provide an accurate description of a random variable if managed with the proper methodology. The Unscented Transform, developed a few years ago, is a method that allows obtaining the statistics of a random variable that undergoes a nonlinear transformation [1]. The method is essentially based on the principle that it is considerably more viable to approximate a Gaussian distribution than to get a proper approximation for an arbitrary nonlinear function or transformation.

The associate editor coordinating the review of this manuscript and approving it for publication was Bora M. Onat.

The UT has been used to develop a generalized Kalman Filter, labeled as Unscented Kalman Filter, which provides better performance, when compared to the traditional Kalman Filter, in nonlinear filters or control applications [1]. Here, the UT has been applied in automotive embedded control systems, particularly in the cases of controlling a DC motor in a mobile seat platform and to a lighting system of heavy-duty vehicles.

Every control system has intrinsic hardware parameters and it is often hard to consider a proper margin for variation that combines their statistical distributions. As an important part of the quality of a project and, consequently, of the product, the research for tools and simulation methods that lead

2169-3536 © 2019 IEEE. Translations and content mining are permitted for academic research only.
Personal use is also permitted, but republication/redistribution requires IEEE permission.
See https://www.ieee.org/publications/rights/index.html for more information.

to failure forecast is justified and still motivates researchers towards more efficient uses of resources and time to market goals.

Several investigations have explored applications using Unscented Transforms (UT) and Monte Carlo (MC) methods. In [12], the Kalman Filter is used to estimate the state of energy and power capacity of ion-lithium batteries, which lead to a 2% error estimation for the parameters. In [13], an improvement of the Kalman Filter was performed, in order to get higher accuracy and make implementation easier, using the idea of avoiding approximations on Taylor Series and predicting mean and covariance up to the third order. An evaluation of the Kalmar filters was performed in [14] for induction sensorless motor drivers, and their non-linear characteristics at low stator speed, resulting in a good performance in predicting driver states. Improvements on variations of Kalman filters and a comparison with Monte Carlo method have been performed in [15] and [16], respectively.

An automotive embedded system comprises several domains from software to hardware. However, in the design and test of the functions at top level one generally neglect uncertainties arising from the electrical and electronic effects, which have unpredictable behavior, and could compromise the device performance even using the appropriate methodology for designing the embedded control system.

In this paper, we demonstrate the applicability of the simulation methods such as Monte Carlo (MC) and Unscented Transform (UT) methods that allow perform analysis of explore the uncertainties in control automotive embedded systems for two application case studies: a Mobile Seat Platform (MSP) and a Light Emitting Diode (LED) used for lighting systems of heavy-duty vehicles. For our studies, the UT demonstrates better performance when compared with MC in which the results allowed identify the following relevant contributions:

i) Definition and comparison of Monte Carlo and Unscented Transform methods for random samples;
ii) Application sample showing the UT effectiveness and likely better performance than Monte Carlo, which could be demonstrated in a real application;
iii) The application and outcome results of UT in two case studies of automotive electrical embedded systems with better performance, justifying its deployment.

This paper is organized as follows: Section II outlines the main characteristics of Monte Carlo and Unscented Transform methods. Section III presents the application sample of UT, such that it could be deployed in the automotive domain. Section IV shows the application of UT in case studies of automotive systems and its better performance, showing its computational feasibility with fewer computer resources and providing outcomes in less time. Finally, Section V discusses the validity and reliability of this methodology applied to those systems being extendible to other embedded systems, in order to be incorporated in a development workflow.

II. BACKGROUND OF MONTE CARLO METHO AND UNCERTAINTY TRANSFORM TO NUMERICAL ANALYSIS

In statistics field, a random sample comprises a subset of samples chosen from a large dataset, in which each sample is chosen randomly and entirely by chance. Each individual has the same probability of being chosen at any stage during the sampling process, and each subset of k samples has the same probability of being chosen for the sample like any other subset of k samples. Therefore, this procedure and technique is well known as a simple random sampling and should not be confused with systematic random sampling.

MC is a well-known method for numeric random analysis that uses repeated random samplings to obtain numerical results for optimization problems, and is often used when analytical solutions are too difficult or impossible.

UT is another method for numeric random analysis. It is a mathematical function used to estimate the result of applying a given nonlinear transformation to a probability distribution that is characterized only in terms of a finite set of statistics. UT is well-known for its use in Unscented Kalman Filter, which uses nonlinear projections of mean and covariance estimates to handle nonlinear systems.

Next, we present the mathematical models of MC and UT.

A. THE MONTE CARLO METHOD

MC can be used to characterize the uncertainty in physical models [2] by sampling a large set of random numbers x_i from a known distribution $p(x)$, and using them as input parameters of the modeled physical system. Once the calculation is completed, the output response statistics can be computed.

This method allows the estimation of all the main statistical characteristics of the output. This is executed by calculating the effect of the system mapping $f(x)$ on a set of random variables x_i. The resulting set of random outputs $y_i = f(x_i)$ are samples of the actual output distribution. This technique is suitable for multiple random variables with multiple probability distributions [2].

The sample mean ($\bar{m}_f$) and variance (s_f^2) of y_i are defined as:

$$\bar{m}_f = \frac{1}{N}\sum_{i=1}^{N} y_i$$
$$s_f^2 = \frac{1}{N-1}\sum_{i=1}^{N}(y_i - \bar{m}_f)^2 \quad (1)$$

They are the unbiased estimates of the real mean m_f and variance σ_f^2 values. As the number of samples increases, the sample mean and variance values converge to the respective real ones. Eq. (1) is also applicable to problems with multiple random variables.

For the determination of the distribution of a continuous random variable, we can define the probability density function (PDF). Then, PDF refers the density of probability rather than the probability mass. Therefore, the concept is

similar to the mass density in physics and its unit is represented by the probability per unit length. To obtain a better perception of PDF, consider a continuous variable such X and define the function $f_X(x)$ as follows such as $f_X(x) = \lim_{\Delta \to 0^+} \frac{P(x<X\leq x+\Delta)}{\Delta}$.

The estimate of the probability density function is obtained with the histogram of the calculated results. The larger the number of samples, the closer the histogram approximates the actual output probability density function.

Given the probability distribution of each variable, it is possible to perform, based on the equations, the generation of random values within the desired range. Each parameter can have a variation determined by a distribution, and its values can be randomly generated, and inserted into the mathematical modeling of the system. The effectiveness of the method depends on a precise equation or modeling (encompassing all the parameters) and on the correct survey of the statistical variation allowed for each parameter [10].

The P parameter has a value within a given range of distribution is the basis of the MC analytical method given in Eq. (2), where F(x) is the distribution function. When there are several variables to be counted in the model, a numerical method is the most appropriate for probability estimation.

$$P = \int_{\sigma 1}^{\sigma 2} \mathrm{F(x)dx} \tag{2}$$

The mathematical model or equation of the system will have a unique output, depending on each randomized value for its parameters. Therefore, the basic principle is to calculate the output variable of the model with a large data set, each with its parameters randomly varied [10].

B. THE UNSCENTED TRANSFORM METHOD

UT refers to a mathematical function that allows estimating the result through the application of a given nonlinear transformation to a probability distribution in terms of a finite set of statistics. It has been developed by Julier and Uhlman [1], with many successful applications [3]–[9].

UT can be described mathematically as a discrete distribution with probabilities p_m (weights) and selected points u_m (sigma points) that could represent a continuous one $p(u)$, where u is a continuous distribution. Therefore, the moments of the discrete u_m must match the moments of the distribution:

$$E\left\{u^k\right\} = \int u^k p\,(u)\,du = \sum u_m^k p_m \tag{3}$$

In general, it is not possible to match all the moments of u. For instance, if one chooses 3 sigma points, there will be 6 equations and, therefore, 6 moments. Naturally, the values of p_m and u_m are directly associated with a continuous distribution $p(u)$ or actually to the moments of this distribution.

The choice of matching the moments is crucial for the accuracy of the UT. The expected value of a random variable u submitted to the mapping $f(u)$ is:

$$E\left\{f\,(u)\right\} = \int f\,(u)\,p\,(u)\,du \tag{4}$$

If the function $f(x)$ can be represented by its Taylor expansion, then a truncated polynomial representation can be written by:

$$f\,(x) = a_0 + a_1 x + a_2 x^2 + \cdots + a_n x^n = \sum_{k=0}^{n} a_k x^k \tag{5}$$

Since this polynomial has an order n, the expected value of the mapping Eq. (4), with a continuous probability density function $p(\hat{u})$, is:

$$\begin{aligned} E\left\{f\,(u)\right\} &= \int \sum_{k=0}^{n} a_k u^k p\,(u)\,du \\ &= \sum_{k=0}^{n} a_k \int u^k p\,(u)\,du \\ &= \sum_{k=0}^{n} a_k E\left\{u^k\right\} \end{aligned} \tag{6}$$

However, with the Unscented Transform, the distribution is discrete, and the expected value is:

$$E\left\{f\,(u)\right\} = \sum p_m f\,(u_m) = \sum_{k=0}^{n} a_k \sum u_m^k p_m \tag{7}$$

where p_m are the weights (probabilities) of the discrete distribution, u_m are the sigma points (discrete points of the distribution). Equation (7) is exact if the number of sigma points is at least $n/2$ on (5). The same idea may be applied to calculate the variance (n sigma points are needed) and other higher moments (more than n sigma points are needed) of the output result. If (5) is only an approximation of the real $f(x)$, then (7) is only an approximation of the real expected value.

As the number of sigma points grows, the discrete distribution tends to a continuous one, although it may not be exactly equal. The same also happens for the output distribution.

C. USING THE UNSCENTED TRANSFORM IN PROBABILITY PROBLEMS

The UT uses the same mathematical formulation as discrete distributions. Therefore, the expected value and variance of a random variable û subjected to a mapping $f(\hat{u})$ is given by:

$$\begin{aligned} E\left\{f\,(u)\right\} &= \bar{F} = \sum p_m f\,(u_m) \\ E\left\{\left(f\,(u) - \bar{F}\right)^2\right\} &= \sum p_m \left(f\,(u_m) - \bar{F}\right)^2 \end{aligned} \tag{8}$$

If there are more random variables, one can represent a joint distribution by combining all discrete distributions if all of them are uncorrelated. The points of the resulting distribution are the combinations of all the sigma points of each distribution, and the probabilities are the product of the probability of the corresponding sigma points, as shown in Fig. 1.

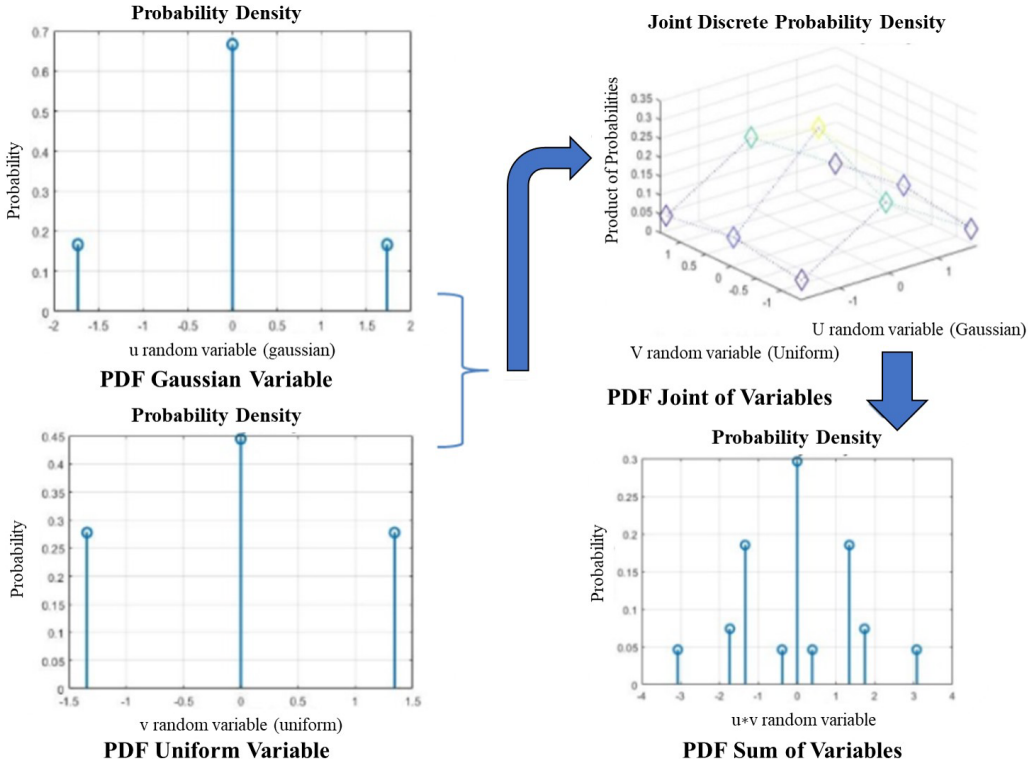

FIGURE 1. Using the UT to represent the sum of two uncorrelated random variables. The joint probability distribution is used to calculate the Probability Density Function (PDF) of the sum of variables (which is the mapping).

If the random variables are correlated, the usual procedure is to use uncorrelated distributions and then obtain new correlated sigma points using the covariance matrix square root between the variables. The procedure is a simple matrix multiplication, in which the inputs are the uncorrelated sigma points.

Considering two uncorrelated random variables and a mapping $f(x,y)$, the expected value and co-variance described in Eq. (8) becomes:

$$E\{f(u,v)\} = \bar{F} = \sum_m \sum_n p_m p_n f(u_m, v_n)$$
$$E\left\{\left(f(u,v) - \bar{F}\right)^2\right\} = \sum_m \sum_n p_m p_n \left(f(u_m, v_n) - \bar{F}\right)^2 \quad (9)$$

The same procedure may be used to calculate the correlation between input and output variables. This is particularly useful, since it is a technique to investigate the relative importance and effect of input variables in the expected result. The correlation between the input and output variables is:

$$\rho_{fu} = \frac{E\left\{\left[f(u,v) - \bar{F}\right][u - E\{u\}]\right\}}{E\left\{[u - E\{u\}]^2\right\} E\left\{[v - E\{v\}]^2\right\}}$$
$$\rho_{fv} = \frac{E\left\{\left[f(u,v) - \bar{F}\right][v - E\{v\}]\right\}}{E\left\{[u - E\{u\}]^2\right\} E\left\{[v - E\{v\}]^2\right\}} \quad (10)$$

III. SAMPLE APPLICATION OF UT

Given the input distribution $p(u)$, the sigma points p_m and weights u_m can be calculated with (3). As an application, we have examined the set of sigma points for the uniform and normal distributions subjected to different nonlinear mappings. The output result is compared to the exact expected value and variance of the mapping.

TABLE 1. Normalized weights p_m and sigma points u_m for uniform or gaussian distributions with different number of sigma points.

		Uniform	Gaussian
2	p_m	$\frac{1}{2}$ $\frac{1}{2}$	$\frac{1}{2}$ $\frac{1}{2}$
	u_m	-1 1	-1 1
3	p_m	$\frac{5}{18}$ $\frac{4}{9}$ $\frac{5}{18}$	$\frac{1}{6}$ $\frac{2}{3}$ $\frac{1}{6}$
	u_m	$-\frac{3}{\sqrt{5}}$ 0 $\frac{3}{\sqrt{5}}$	$-\sqrt{3}$ 0 $\sqrt{3}$
4	p_m	$\frac{18-\sqrt{30}}{72}$ $\frac{18+\sqrt{30}}{72}$ $\frac{18+\sqrt{30}}{72}$ $\frac{18-\sqrt{30}}{72}$	$\frac{3-\sqrt{6}}{12}$ $\frac{3+\sqrt{6}}{12}$ $\frac{3+\sqrt{6}}{12}$ $\frac{3-\sqrt{6}}{12}$
	u_m	$-\sqrt{\frac{45+6\sqrt{30}}{35}}$ $-\sqrt{\frac{45-6\sqrt{30}}{35}}$ $-\sqrt{\frac{45-6\sqrt{30}}{35}}$ $-\sqrt{\frac{45+6\sqrt{30}}{35}}$	$-\sqrt{3+\sqrt{6}}$ $-\sqrt{3-\sqrt{6}}$ $\sqrt{3-\sqrt{6}}$ $\sqrt{3+\sqrt{6}}$

Table 1 shows the Sigma points and weights for the uniform and Gaussian (zero mean and unitary variance) distributions. These are normalized Sigma points, which means

TABLE 2. Analytical and UT outcomes for the mapping $f(x) = 2 - 3x + 4x^2$ with different numbers of sigma points.

	Uniform		Gaussian	
	Mean	Variance	Mean	Variance
	Analytical: 70	Analytical: $\frac{17844}{5}$	Analytical: 70	Analytical: 3876
2	70	3364	70	3364
3	70	$\frac{17844}{5}$	70	3876
4	70	$\frac{17844}{5}$	70	3876

TABLE 3. Analytical and results for the mapping $f(x) = 3\cos\frac{x}{2}$, with different number of sigma points.

	Uniform		Gaussian	
	Mean	Variance	Mean	Variance
	Analytical: -0.711	Analytical: 4.263	Analytical: -0.757	Analytical: 3.529
2	-0.711	4.263	-0.757	3.529
3	-0.675	5.269	-0.675	5.269
4	-0.712	4.151	-0.766	2.883

that they should be denormalized to be applied in regular problems, which is performed by multiplying the Sigma points by the standard deviation of the denormalized distribution and adding the result to the distribution mean.

As an example, consider a random variable x with mean $E(x) = 4.0$ and standard deviation $\sigma = 2.0$. The new sigma points are calculated using $4.0 + 2.0\,u_m$. Using the new sigma points and weights in Table 1, which were applied to two different mappings $f(x)$. The first is a simple polynomial $f(x) = 2 - 3x + 4x^2$, and the second the function $f(x) = 3\cos\frac{x}{2}$. Table 2 shows very accurate results for the polynomial mapping. This is a direct consequence of Eq. (8), which states that such mappings will be as exact as the number of Sigma points represent the order of the resulting polynomial. This also explains why the variance for the two sigma-point schemes is inexact since the variance is given by $E\left\{f^2(x)\right\} - E\{f(x)\}^2$. The resulting fourth-order mapping polynomial is not adequately represented by the two sigma-point scheme. However, the three- and four-point schemes support polynomials of much higher order.

Table 3 shows the UT behavior if the mapping is nonpolynomial. As the number of Sigma points increases, the polynomial natural of UT provides a better representation of the actual mapping. However, the table also shows that convergence also depends on the PDF.

IV. CASE STUDY

We present two application studies on the effect of uncertainty in the automotive domain, comparing MC and UT, including the Mobile Seat Platform (MSP), and the Light Emitting Diode (LED) used for lighting systems of heavy-duty vehicles.

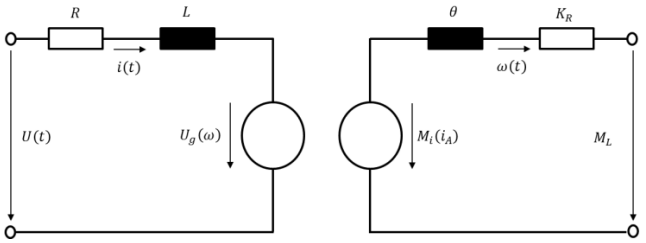

FIGURE 2. DC-Motor electromechanical system.

A. MOBILE SEAT PLATFORM

A MSP automation facility project has been developed to improve accessibility to people with disabilities in public transportation vehicles [10]. The MSP comprises a reversible DC motor, controlled by a simple switch manual device, which controls the platform motion where the seat is fixed. A more detailed analysis of the load behavior requires the electromechanical circuit of the DC-Motor. This may be performed analytically, based on the representation of Fig. 3.

The load torque M_L value was obtained by measuring with a standard load of 75 kg, added to the weight of the platform (50 kg) and the seat (25 kg). Applying circuit theory, to the model of Fig. 2, results in two coupled differential equations, respectively one for the electrical subsystem, and the other for the mechanical subsystem:

$$\begin{aligned} L\frac{di(t)}{dt} + Ri(t) + U_g(\omega(t)) &= U(t) \\ J\frac{d\omega(t)}{dt} + K_r\omega(t) - M(i(t)) &= -M_L \end{aligned} \tag{11}$$

where the constants are defined in Table 4.

TABLE 4. Electrical motor parameters.

Symbol	Description	Unit	Value
$U(t)$	Electric input terminal voltage	V	27
$i(t)$	Armature electrical current	A	Variable
$\omega(t)$	Rotational frequency	1/s	Variable
R	Motor series resistance	Ω	0.39
k	Generator constant	V.s	0.6
L	Motor Inductance	H	0,001
J	Moment of inertia	Kgm^2	0.075
K_R	Sliding friction constant	Nms	20
M_L	Load torque	Nm	18

Utilizing the linear approximation, back electromagnetic force equals to velocity constant versus rotational velocity of the armature ($U_g(\omega(t)) = kv.\omega$). On the mechanical side, $M(i)$ is the mechanical torque, which can be written as torque constant versus armature current ($M(i) = kt.i$). The velocity and toque constant is related to the same parameters (flux density of magnets, reluctance of iron core and number of windings), which take place in the analogy used on electromechanical transformation of energy (mechanical velocity to electrical current), and so the same constant is represented

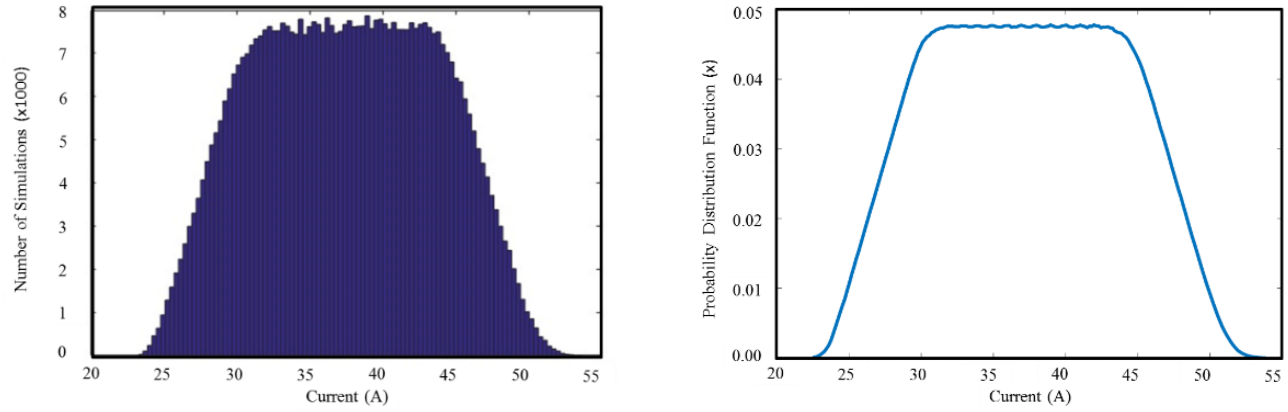

(a) (b)

FIGURE 3. Permanent current probability density function estimate: (a) Monte Carlo histogram and (b) Unscented Transform probability density function.

as 'k'. Consequently, the DC-Motor electromechanical system has the dynamics representation described by Eq. (11), which could be updated by the following Eq. (12) with the constant k on the left side of both differential equations.

$$\begin{aligned} L\frac{di\,(t)}{dt} + Ri\,(t) + k\omega\,(t) &= U \\ J\frac{d\omega\,(t)}{dt} + K_r\omega\,(t) - ki\,(t) &= -M_L \end{aligned} \tag{12}$$

The differential equations described in Eq. 12, are on time domain and are hard to solve analytically. Therefore, we can use the Laplace Transform method that allows takes a function of a real variable t (often time) to a function of a complex variable s (complex frequency). That allows solving linear differential equation with given initial conditions. The steps to apply are: given a differential equation, we have to apply Laplace Transform ($\mathcal{L}$) to transform in the frequency domain in order to perform operations and isolate the variable (s), in which we need to find out the dynamic response. Finally, we apply the inverse Laplace Transform ($\mathcal{L}^{-1}$) to transform from the frequency domain to the time domain achieving the solving of the differential equation in the time domain.

$$\begin{aligned} LsI\,(s) + RI\,(s) + k\Omega\,(s) &= U \\ Js\Omega\,(s) + K_r\Omega\,(s) - kI\,(s) &= -M_L \end{aligned} \tag{13}$$

Hence,

$$I\,(s) = \frac{\left(\dfrac{U}{s} + \dfrac{kM_L}{J}\dfrac{1}{\left(s + \dfrac{kr}{J}\right)s}\right)(kR + sJ)}{LJs^2 + s\,(RJ + Lkr) + k^2} \tag{14}$$

The time-domain current $I(t)$ is obtained after inverse Laplace transform, shown in Eq. (14). The permanent current is determined by M_L/k ratio, given that the exponential components tend to zero as time runs.

$$\begin{aligned} I\,(t) = \frac{ML + kr}{k} + \frac{1}{4kr^2k^2\omega_0}\left(\left(\frac{2k^2}{L} - \frac{kr^2}{J} - \frac{Rkr}{L}\right)U\right. \\ \left. + \left(\frac{R}{L} - \frac{k^2r}{J}\right)ML\right)e^{-\alpha t}\sinh\left(\omega_0 t\right) \\ - \left(U\frac{kr}{k^2} + k\frac{ML}{k}\right)\cosh\left(\omega_0 t\right)e^{-\alpha t} \end{aligned} \tag{15}$$

where:

$$\omega_0 = \sqrt{\alpha^2 - \frac{k^2}{LJ}} \quad \text{and } \alpha = \frac{R}{2L} + \frac{kr}{2J}$$

Usually, there are statistical variations on the parameters of the model. This allowed to define the percentage variation of each parameter that is expected (based on the production history), although it was not possible to determine the statistical function that controls each parameter:

- R: variability is $\pm$ 7% due to construction, and + 19.5% due to temperature (increase up to 50K). Therefore, the change from -7% to + 19.5% is considered;
- Magnetic properties (L and J): 8% (due to manufacturing);
- Torque constant (k): -5% (increase of 50K in temperature);
- Constant slip: + 5% for given speed with free rotor (no load).
- As the MSP never operates without load (there is always the weight of the platform and the armchair), it will not be considered a variable parameter;
- The typical supply voltage range is [18V, 32V], but since the engine does not operate below 21 V, we assume the range of [18V, 32V] instead;
- The weight varies between empty (75 kg) and a maximum weight of 200 kg (design limit). There is a direct relationship between weight and effort made be electric motor given in Newton Meter (Nm) and measured through the current. The variation goes from 9 to 24 Nm.

Given the variable ranges, the next step is to define a function to generate random values for each variable within its range. We assume the uniform distribution for each parameter, in the absence of any other knowledge from the

TABLE 5. Comparison of permanent current.

Permanent Current	MC (500000 tests)	UT (729 tests)	UT (15625 tests)
Mean	37.52	37.41	37.52
Standard Deviation	6.12	6.12	6.12

manufacturer. Table 4 presents the relevant average motor parameters for the circuit model of Fig. 3.

We both MC and UT to calculate the uncertainty of the total model. Table 5 shows the mean and standard deviation of the permanent current are presented in.

The Probability Density Function is also available from Monte Carlo and UT. In Monte Carlo, the histogram presents the general shape of the resulting distribution, while the UT demands more laborious calculations of the general mapping. The pdf is represented as a histogram with MC, while the UT demands more laborious calculations of the general mapping. The results are presented in Fig. 3. OK Fig. 3 shows a comparison between MC and UT applied to the MSP. UT is very efficient, and only requires a fraction of the computing resources used by MC. Table 5 shows how many tests were necessary in the UT and Monte Carlo. The main difference is that, while Monte Carlo used a large number of random variations of the input parameters, the UT only needed a selected deterministic number of them to achieve similar results (such as shown in Table 1). The calculation of the probability density function with the UT instead of the histogram of the Monte Carlo analysis is another advantage of the method, assembled by polynomial approximation of the nonlinear mapping.

After all parameters are defined with a random generation function, the next step is to define the literal Eq. (15) in Matlab (right side of the command lines). This equation will return a single value of I for one single set of parameters (ex.$V = 27.6V$, ML=10.5N.m, R = 0.41Ω etc), in function of time (t). If we interested in knowing which one is the highest current value, a filter to save the highest value for each time step (n = n° of simulations) can be set. The Algorithm 1 shows how to create the random generation function.

B. IGHT EMITTING DIODE

We consider the LED in terms of the life-cycle estimation [11]. The lighting systems of heavy-duty vehicles, such as trucks, buses, and trains, used to be of fluorescent lamps and inverters, which have been replaced by the LED, thanks to its many advantages such as long lifetime, energy efficiency, durability, no emission, operational at high temperatures, dispersion, high frequency of switching, and low voltage. We evaluate the mean junction temperature of a LED lighting system, which is directly correlated to the mean lifetime of the system.

The topology of the mechanical structure of the LED is shown in Fig. 4 [11].

Algorithm 1 Random Generation Function

```
Setup Parameters
V=unifrnd(21,32);
k=unifrnd(0.57,0.6);
L=unifrnd(9,24);
J=unifrnd(0.069,0.081);
L=unifrnd(0.00092,0.00108);
R=unifrnd(0.3627,0.466);
Algorithm
Begin
    Imax=0;
    for t=0.01:10
        I = equation (6);
        if(I>Imax)
            Imax = I;
        end
    end
    Ipeak(n)=Imax;
End
```

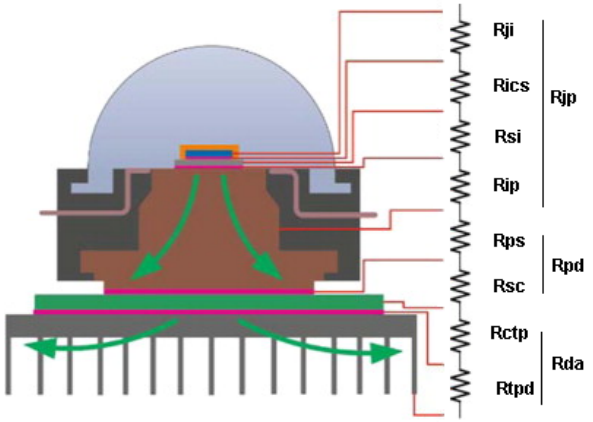

FIGURE 4. LED internal and external assembly topology.

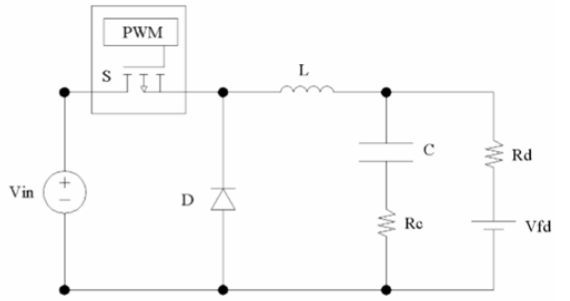

FIGURE 5. DC-DC power electronic supply model with PWM controlled switch.

The LED junction temperature is given by T_j is shown in Eq. (16), easily found in power electronics books such as [11]. The concept leads to the sum of all thermal resistance of every material connection, multiplied by the total power P conducted in the LED, to result in a temperature difference $T_j - T_{pad}$ between junction and pad. This comes from a basic analogy of the thermal equation of heat flow ($R_{th} = \frac{\Delta T}{Q}$, where ΔT is the temperature difference, Q is the heat flow, and R_{th} is the thermal resistance given by the distance that

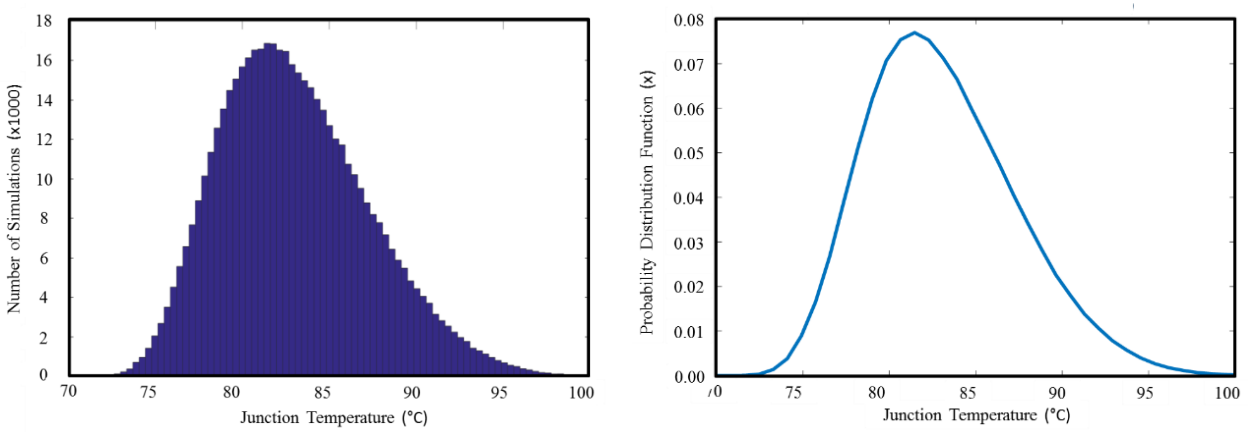

(a) (b)

FIGURE 6. MC vs. UT for Junction temperature in the LED application.

the heat flows, divided by the thermal conductivity versus area) with the Ohm's law ($R_e = \frac{\Delta V}{I}$). In this analogy, Q is equivalent to power dissipation.

$$T_j = T_{pad} + P\left(R_{jp} + R_{pd} + R_{da}\right) \tag{16}$$

The thermal resistances are defined such:

- R_{ji} : between junction and interconnection layer;
- R_{ics} : between interconnection layer and ceramic substrate;
- R_{csi} : between ceramic substrate and another interconnect layer;
- R_{ip} : between interconnect layer and pad;
- R_{ps} : between pad and solder joint layer;
- R_{sc} : between solder joint and copper (trace);
- R_{ctp} : between copper and thermal paste;
- R_{tpd} : between thermal paste and external heatsink.

where T_{pad} is pad temperature; $R_{pd}$is the pad and dissipation layer resistance; R_{jp} is a combination of other parameters, and should be given in the datasheet; R_{da} is the dissipation layer and air resistance, calculated by (17).

$$R_{da} = \frac{3.3 * Cf}{4 * w * \sqrt{\lambda}} + \frac{650 * Cf}{A} \tag{17}$$

- C_f: Correction coefficient regarding to the type of material (dark or brilliant) and the position at the board (vertical or horizontal). For a brilliant material on horizontal direction, this coefficient is 1;
- λ: Copper thermal expansion coefficient, $3.85W/°$ C.cm;
- w: copper thickness. Designed to be 1mm, with manufacturer tolerance of $\pm$0.05mm;
- A: copper area, designed as $26 \times 99\text{mm}^2$, 0.2mm^2 tolerance.

The power parameter P is obtained by (18) and (19), as shown at the bottom of this page.

Fig. 5 shows the switched mode step down Buck converter used as the LED power supply. V_{in} is the battery supply available from the vehicle; S is a PWM (Pulse Width Modulation) controlled switch; D and L are respectively a diode (on when the switch is off) and an inductor (charging when the switch is on); the output capacitance filter is represented by C and its series resistance R_c. The load is the LED, modeled as a constant power supply and a resistance V_{fd}. The converter works as follows: when the switch is closed, the battery V_{in} charges the inductor, capacitance and feeds the load. When the switch is off, the inductor and capacitor keep the load current, which discharges gradually through the diode. (The PWM circuit for the switch is omitted in the figure.) The main objective of the converter is to keep the load current constant by changing the PWM duty cycle, which is increased if V_{in} is decreased, and decreased V_{in} is increased. The transference function is shown in (18), and the LED power is shown in (19) [11].

We assume uniform distribution unless otherwise noted:

- C: Buck Converter Output Capacitance, variability is $\pm$ 10%;
- L: Buck Converter Inductance, variability is $\pm$ 5%;
- R_C: Capacitor series resistance, variability between 3.58 and 7.56 mΩ;
- T_{pad}: PAD temperature, variability between 62.11 and 66.11 °C;

$$I_{LED} = \left[\frac{V_{in}D\left(1 + s\left(\frac{L + CR_dR_c}{R_d}\right) + s^2LC\left(1 + \frac{R_c}{R_d}\right)\right)}{R_d(1 + sCR_c)} - \frac{V_{fd}}{R_d}\right] \tag{18}$$

$$P = V_{fd}I_{LED} + R_dI_{LED}^2 \tag{19}$$

TABLE 6. Comparison of junction temperature outcomes for monte carlo and unscented transform.

Junction Temperature	Monte Carlo (500000 tests)	Unscented Transform (19693 tests)
Mean	83.04	83.03
Median	82.59	82.62
Standard Deviation	4.30	4.30

TABLE 7. Parameter effect in power dissipation.

Parameter	Variable Range	Correlation	% total variance
C (buck converter output capacitance)		-0.7	50
L (buck converter inductance)		-0.35	12
T_{pad} (P_{ad} Temperature)		0.27	7
V_{fd} (LED mean direct voltage)		0.41	17
R_{jp} (thermal junction-pad resistance)		0.35	12

- R_{tpd}: Mean thermal pad resistance, variability between 0.13 and 0.15 °C/W;
- Wt: Strip width, variability between 0.095 and 1.05 mm;
- A: Strip area, variability between 2573.96 and 2574.04 mm^2;
- V_{fd}: Direct diode voltage, variability between 2.5 and 3.99 V;
- R_{jp}: Thermal junction-PAD resistance, normal distributions with mean 10.3 and 0.9 standard deviation ($°C/W$).

We used MC and UT to calculate the uncertainty of the junction temperature. The mean and a standard deviation of the junction temperature is presented in Table 6.

The results are presented in Fig. 6 and show respectively the distribution of the number of simulations performed and the probability distribution function.

The UT also allows an estimation of the influence of each input variable in the final result. This is a covariance analysis. A careful analysis could determine which variables are most relevant to the mathematical model. Table 7 shows that the increase of the filter capacitance leads to a decrease in the junction temperature.

The UT probability distribution function compares very well with the Monte Carlo histogram. Additionally, the correlation between input and the junction temperature indicates that the Buck Converter Capacitance is the leading factor in the junction temperature, followed by the mean direct voltage, the thermal junction-PAD resistance, and the PAD temperature. The UT analysis indicates that these are the main variables needed to model appropriately the variability in the diode example.

V. CONCLUSION

In this paper, we compare MC and UT as statistical tools to improve simulation performance in automotive embedded control systems. We have used those methods in two examples that show the flexibility and scope of the approach: a mobile seat platform and a LED-based lighting system. In both cases, the UT used only a small amount of the resources needed for the Monte Carlo analysis. This a natural feature of the UT. In the LED case, the UT was used to estimate the probability density function (similar to the Monte Carlo histogram), as well as a correlation analysis. The UT provided information that could potentially allow the reduction of the model needed for statistical characterization.

REFERENCES

[1] S. J. Julier and J. K. Uhlmann, "Unscented filtering and nonlinear estimation," *Proc. IEEE*, vol. 92, no. 3, pp. 401–422, Mar. 2004.

[2] A. Papoulis, *Probability, Random Variables, and Stochastic Processes*, 3rd ed. New York, NY, USA: McGraw-Hill, 1991.

[3] S. J. Julier and J. K. Uhlmann, "A consistent, debiased method for converting between polar and Cartesian coordinate systems," in *Proc. SPIE, AeroSense, Acquisition, Tracking Pointing XI*, vol. 3086, 1997, pp. 110–121. [Online]. Available: https://link.springer.com/chapter/10.1007/11890348_24 and https://www.spiedigitallibrary.org/conference-proceedings-of-spie/3086/0000/Consistent-debiased-method-for-converting-between-polar-and-Cartesian-coordinate/10.1117/12.277178.short?SSO=1

[4] S. J. Julier, "Comprehensive process models for high-speed navigation," Ph.D. dissertation, Univ. Oxford, Oxford, U.K., Oct. 1997.

[5] S. J. Julier and J. K. Uhlmann, "A general method for approximating nonlinear transformations of probability distributions," Dept. Eng., Univ. Oxford, Oxford, U.K., Tech. Rep. 16784239, 1996. [Online]. Available: http://www.robots.ox.ac.uk/~siju/work/w and https://www.semanticscholar.org/paper/A-General-Method-for-Approximating-Nonlinear-of-Julier-Uhlmann/523a865ffabb50d10f85d141963d40528e952760

[6] S. J. Julier, "The spherical simplex unscented transformation," in *Proc. Amer. Control Conf.*, vol. 3, Jun. 2003, pp. 2430–2434.

[7] J. L. Crassidis and F. L. Markley, "Unscented filtering for spacecraft attitude estimation," *J. Guid., Control, Dyn.*, vol. 26, no. 4, pp. 536–542, Jul. 2003.

[8] L. Sige, Z. Xiaoxin, F. Mingtian, and Z. Zhuping, "Probabilistic power flow calculation using sigma-point transform algorithm," in *Proc. PowerCon*, Oct. 2006, pp. 1–5.

[9] L. D. Menezes, A. Ajayi, C. Christopoulos, P. Sewell, and G. A. Borges, "Efficient computation of stochastic electromagnetic problems using unscented transforms," *IET Sci., Meas. Technol.*, vol. 2, no. 2, pp. 88–95, 2008.

[10] L. Nunes, M. Santos, J. Neme, R. Rodrigues, and K. Collazos, "The Monte Carlo method for non-detected failure analysis on dynamic systems testing," in *Proc. 43rd Annu. Conf. IEEE Ind. Electron. Soc. (IECON)*, Beijing, China, Oct./Nov. 2017, pp. 5084–5089.

[11] L. R. Nunes, M. M. Santos, K. S. Collazos, and R. K. Keshri, "Thermal uncertainty simulation on LED lighting boards of heavy duty transportation vehicles," in *Proc. 44rd Annu. Conf. IEEE Ind. Electron. Soc. (IECON)*, Washington, DC, USA, Oct. 2018, pp. 2157–2162.

[12] W. Zhang, W. Shi, and Z. Ma, "Adaptive unscented Kalman filter based state of energy and power capability estimation approach for lithium-ion battery," *J. Power Sources*, vol. 289, pp. 50–62, Sep. 2015.

[13] S. Julier, J. Uhlmann, and H. F. Durrant-Whyte, "A new method for the nonlinear transformation of means and covariances in filters and estimators," *IEEE Trans. Autom. Control*, vol. 45, no. 3, pp. 477–482, Mar. 2000.

[14] S. Jafarzadeh, C. Lascu, and M. Fadali, "State estimation of induction motor drives using the unscented Kalman filter," *IEEE Trans. Ind. Electron.*, vol. 59, no. 11, pp. 4207–4216, Nov. 2012.

[15] H. M. T. Menegaz, J. Y. Ishihara, G. A. Borges, and A. N. Vargas, "A Systematization of the Unscented Kalman Filter Theory," *IEEE Trans. Autom. Control*, vol. 60, no. 10, pp. 2583–2598, Oct. 2015.

[16] J. E. G. de Medeiros, S. A. P. Haddad, and L. R. A. X. de Menezes, "Extended formulation for unscented transform and its application as Monte Carlo alternative," *IEEE Electron. Lett.*, vol. 52, no. 22, pp. 1842–1843, Oct. 2016.